

**A determination of  $H_0$  with the CLASS gravitational lens  
B1608+656:**

**II. Mass models and the Hubble constant from lensing.**

L. V. E. Koopmans

Kapteyn Astronomical Institute, University of Groningen,  
P.O.Box 800, NL-9700 AV Groningen, The Netherlands  
e-mail: leon@astro.rug.nl

and

C. D. Fassnacht<sup>1</sup>

California Institute of Technology  
105-24, Pasadena CA 91125, USA  
e-mail: cdf@astro.caltech.edu

Received : 1999 April 7;    accepted : 1999 July 1

---

<sup>1</sup> Current Address: NRAO, P.O. Box O, Socorro, NM 87801. Current e-mail: cfassnac@aoc.nrao.edu

## ABSTRACT

We present mass models of the four-image gravitational lens system B1608+656, based on information obtained through VLBA imaging, VLA monitoring and *Hubble Space Telescope* (HST) WFPC2 and NICMOS imaging. A mass model for the lens galaxies has been determined that reproduces (i) all image positions within the observational errors, (ii) two out of three flux-density ratios within about 10% from the observed ratios and (iii) the model time delays within 1% from their observed values, given our best estimate of the Hubble parameter.

Using the time delays determined by Fassnacht et al. (1999a), we also find that the best isothermal mass model gives  $H_0 = 59_{-6}^{+7}$  km s<sup>-1</sup> Mpc<sup>-1</sup> for  $\Omega_m = 1$  and  $\Omega_\Lambda = 0.0$ , or  $H_0 = (65 - 63)_{-6}^{+7}$  km s<sup>-1</sup> Mpc<sup>-1</sup> for  $\Omega_m = 0.3$  and  $\Omega_\Lambda = 0.0-0.7$ . The statistical errors indicate the 95.4% ( $2\text{-}\sigma$ ) confidence interval. A systematic error of  $\pm 15$  km s<sup>-1</sup> Mpc<sup>-1</sup> is estimated from a 20% ( $1\text{-}\sigma$ ) uncertainty in the steepness of radial mass profile.

This cosmological determination of  $H_0$  agrees well with determinations from three other gravitational lens systems (i.e. B0218+357, Q0957+561 and PKS1830-211), Type Ia Supernovae, the Sunyaev-Zel'dovich effect and local determinations. The current agreement on  $H_0$  – within the  $1\text{-}\sigma$  statistical errors – from four out of five gravitational lens systems (i) emphasizes the reliability of its determination from isolated gravitational lens systems and (ii) suggests that a close-to-isothermal mass profile can describe disk galaxies (e.g. B0218+357 and possibly PKS1830-211), ellipticals (e.g. B1608+656) and central cluster ellipticals (e.g. Q0957+561).

The average of  $H_0$  from B0218+357, Q0957+561, B1608+656 and PKS1830-211, gives  $H_0^{\text{GL}} = 69 \pm 7$  km s<sup>-1</sup> Mpc<sup>-1</sup> for a flat universe with  $\Omega_m = 1$  or  $H_0^{\text{GL}} = 74 \pm 8$  km s<sup>-1</sup> Mpc<sup>-1</sup> for  $\Omega_m = 0.3$  and  $\Omega_\Lambda = 0.0-0.7$ . When including PG1115+080, these values decrease to  $64 \pm 11$  km s<sup>-1</sup> Mpc<sup>-1</sup> and  $68 \pm 13$  km s<sup>-1</sup> Mpc<sup>-1</sup>, respectively. The errors are the estimated  $2\text{-}\sigma$  errors on the average. The Hubble parameter from gravitational lenses seems to agree best with local determinations of  $H_0$  for a low density universe, under the assumption that all lenses are nearly isothermal.

*Subject headings:* cosmology: gravitational lensing – dark matter – distance scale

## 1. Introduction

Since the discovery of the first gravitational lens Q0957+561 (Walsh, Carswell & Weymann 1979), there has been considerable interest in monitoring the radio and optical emission of its lens images (a quasar at  $z = 1.41$ ), in order to find correlations between their light curves. Strong correlations can give a time delay between the images and definitively prove that they are lensed images of one background object. Already in 1964 it was shown that such a time delay can be used to constrain the Hubble parameter ( $H_0$ ), if a good lens mass model can be found (Refsdal 1964).

For Q0957+561 several long-term monitoring programs finally resulted in a robust determination of the time delay (e.g. Kundić et al. 1997b). Combined with the lens mass model a value of  $H_0 = 63 \pm 12$  km s<sup>-1</sup> Mpc<sup>-1</sup> (95% confidence) was determined (Kundić et al. 1997b). However, a new interpretation of the data shed some doubt on the reliability of the confidence levels quoted for the mass models (Barkana et al. 1998), and a new determination the velocity dispersion of the cluster lens by Tonry & Franx (1999) increased the value of  $H_0$  to  $70 \pm 7$  or  $72 \pm 7$  km s<sup>-1</sup> Mpc<sup>-1</sup> ( $1-\sigma$ ), using the SPLS or FGS models from Grogin & Narayan (1996a, 1996b), respectively. All values of  $H_0$  are given for a flat universe with  $\Omega_m=1$ , if not specified otherwise.

Three other gravitational lens systems have also yielded values of  $H_0$ . From the gravitational lens PG1115+080 (Weymann et al. 1980) a value of  $H_0 = 44 \pm 4$  km s<sup>-1</sup> Mpc<sup>-1</sup> ( $1-\sigma$ ) was determined (Impey et al. 1997) using the time delays found by Schechter et al. (1997) and an isothermal lens mass model. The gravitational lens system resides near a compact group of galaxies (Kundić et al. 1997a; Tonry 1998), which complicates the mass model considerably.

The time delay in B0218+357 (e.g. Patnaik et al. 1993) was recently determined by Biggs et al. (1999) to within 4% accuracy (95% confidence). This significantly reduced the uncertainty compared with a previous determination by Corbett et al. (1996). Preliminary modeling of this system gave  $H_0 = 69^{+13}_{-19}$  km s<sup>-1</sup> Mpc<sup>-1</sup> (95% confidence), using an isothermal mass model to describe the lens galaxy (Biggs et al. 1999).

Very recently the time delay in PKS1830-211 (e.g. Jauncey et al. 1991) was determined (Lovell et al. 1998). Combined with the detailed mass model from Nair, Narasimha & Rao (1993) and the source redshift found by Lidman et al. (1998), a value of  $H_0=65^{+16}_{-9}$  km s<sup>-1</sup> Mpc<sup>-1</sup> ( $1-\sigma$ ) was determined (Lovell et al. 1998; Lovell, private communication). When using an isothermal mass model on the galaxy position from Nair et al. (1993) we estimate  $H_0=75^{+18}_{-10}$  km s<sup>-1</sup> Mpc<sup>-1</sup> ( $1-\sigma$ ).

Using the same lens mass model for all five gravitational lens systems makes a more consistent comparison of  $H_0$  from these systems possible (Schechter 1998), especially if their radial mass profile is ill-constrained. We have chosen to use the isothermal mass model.

In sections 2 and 3 we will briefly discuss the observational status of B1608+656 and new observations that are used in this paper. Section 4 introduces the mass distribution and the procedure that is used to solve for the mass model parameters and the Hubble parameter. In section 5, the results for different mass models are presented. In section 6, a determination of the Hubble parameter from B1608+656 is given. In section 7 this estimate is compared with determinations from other gravitational lens systems and in section 8 with determinations from Type Ia Supernovae and the Sunyaev-Zel'dovich effect and the local determination of  $H_0$ . The conclusions are summarized in section 9.

The observed time delays between the lens images in B1608+656 are presented in the companion paper by Fassnacht et al. (1999a; hereafter Paper I).

## 2. The four-image gravitational lens B1608+656

The four-image gravitational lens system B1608+656 was discovered by the *Cosmic Lens All Sky Survey* collaboration (CLASS; Myers et al. 1995; Myers et al. 1999, in preparation) and independently by Snellen et al. (1995).

The goal of CLASS is to compose a statistically complete sample of radio-selected gravitational lenses, for which the selection effects are well understood (Browne et al. 1997). For this purpose all flat-spectrum ( $\alpha < 0.5$  with  $S_\nu \propto \nu^{-\alpha}$ ) radio sources brighter than 25 mJy at 5 GHz were selected between declinations 0 and 75 degrees (Browne et al. 1997). These sources ( $\approx 12,000$  in total) were observed with the VLA in A-array at 8.4-GHz. Promising lens candidates were followed-up with MERLIN and/or the VLBA. So far at least 12 new gravitational lens systems were found (e.g. Jackson et al. 1998; Browne et al. 1997).

The lensed object in B1608+656 is the nucleus of radio galaxy at a redshift  $z_s = 1.394$  (Fassnacht et al. 1996) which has a radio luminosity in the transition range between Fanaroff-Riley Class I and II galaxies (Fanaroff & Riley 1974, Snellen et al. 1995; Fassnacht et al. 1996). The primary lens galaxy has a redshift  $z_l = 0.6304$  (Myers et al. 1995). Additional multi-frequency observations with several radio telescopes (VLA, MERLIN, VLBA) and HST were done. The relevant results will be summarized in section 3.

Flat-spectrum radio sources are often variable. This is one of the prerequisites for determining the time

delay between lens images and constraining  $H_0$  (Refsdal 1964). The lensed object in B1608+656 is compact and has varied  $\approx 20\%$  in flux density (8.4-GHz) on time scales of weeks to months (Fassnacht 1997). Thus, a seven-month monitoring campaign was started with the VLA in A- and B-arrays during the 1996–1997 season to determine time delays between the image-pairs (Paper I). The obtained time delays, flux density ratios and additional radio and optical data from B1608+656 will be used in this paper to constrain the mass model of this gravitational lens system, culminating in an estimate of the Hubble parameter.

### 3. Data

Most of the observations and data summarized in this section will be presented in Fassnacht et al. (1999b, in preparation). The image light curves, time delays and flux density ratios from the VLA 8.4-GHz monitoring campaign are presented in the companion paper (Paper I).

#### 3.1. Image positions

From deep VLBA 5-GHz observations of B1608+656 very precise relative positions of the four lens images were obtained (Fassnacht et al. 1999b, in preparation). The results are listed in Table 1. The four images are compact and show no extended structure on scales  $\gtrsim 1$  mas. Data reduction and image fitting was done in the NRAO data reduction package *AIPS*. The statistically expected errors on the image positions are approximately the FWHM of the restoring beam divided by the signal-to-noise of the component (Table 1).

#### 3.2. Flux density ratios and time delays

The light curves of the four lens images can give (i) the time delays, if correlations between the light curves are found, and (ii) the ‘true’ flux density ratios between the lens images, after correction for the time delays.

The exact procedure and results from the VLA 8.4-GHz monitoring campaign of B1608+656 are described in the companion paper (Paper I). In Table 1, we list the obtained results. We use the flux density ratios and time delays to constrain the lens mass models of B1608+656. The errors on the time delays are between 12% and 23% ( $2\text{-}\sigma$ ), determined from Monte-Carlo simulations (Paper I).

Image	A	B	C	D
$x_i^o$ (")	$\equiv 0.0000$	-0.7380	-0.7446	+1.1284
$y_i^o$ (")	$\equiv 0.0000$	-1.9612	-0.4537	-1.2565
$\delta x_i$ (mas)	0.0023	0.0043	0.0045	0.0107
$\delta y_i$ (mas)	0.0023	0.0046	0.0049	0.0124
$r_i^o = S_\nu^i / S_\nu^A$	$\equiv 1.000$	0.490	0.508	0.172
$\delta r_i$	$\equiv 0.000$	0.020	0.020	0.020
$t_i^o$ (d)	30	$\equiv 0$	36	76
$\delta t_i$ (d)	+7/-7	$\equiv 0$	+7/-7	+9/-10

Table 1: Properties of the radio lens images of B1608+656. The positions were determined from VLBA observations (Fassnacht et al. 1999, in preparation). The coordinate system is Cartesian with the positive  $x$ -axis pointing west. The errors are the formal  $1\text{-}\sigma$  errors (FWHM of the beam divided by the signal-to-noise) from the VLBA data. The flux density ratio and time delays were determined from the VLA monitoring observations (Paper I). The errors on the time delays (95% confidence) were determined from Monte-Carlo simulations. The errors on the flux density ratios are assumed larger than the formal Monte-Carlo errors for reasons given in section 3.2.

The errors on the flux density ratios are about 0.002, determined from the same Monte-Carlo simulations. Systematic differences between the light curves, however, appear appreciably larger than the error on the individual light-curve points, because the reduced  $\chi^2$  between the light curves is always significantly larger than unity (Paper I). Because the flux density ratios are most sensitive to small changes in the lens potential (e.g. milli-lensing, micro-lensing in the case of a very compact source ( $\ll 1$  mas), the presence of small nearby companions to the lens galaxies, etc.), small-scale scintillation or systematic self-calibration errors, we will conservatively assume an error of 0.02 on the flux density ratios, which is approximately the scatter between the individual points of each light curve. In Koopmans & de Bruyn (1999, in preparation) it is shown that a few percent variability in radio light curves at 8.4-GHz can be expected for weak flat-spectrum radio sources, due to micro-lensing. A few-percent error on the flux-density ratios is already a considerable improvement on the 20% error used in previous models (e.g. Keeton & Kochanek 1997).

### 3.3. The lens galaxies

*Hubble Space Telescope* (HST) exposures were obtained of B1608+656, both with the WFPC2 (F555W and F814W) and NICMOS (F160W). The F814W exposure of B1608+656 is presented in Jackson et al. (1998) and Fassnacht et al. (1999b, in preparation). The F555W and F160W exposures will be presented in Fassnacht et al. (1999b, in preparation).

All three exposures show four optical lens images and two objects confined in the region between the lens images. These objects remain distinctly separated in the F555W, F814W and F160W exposures. We assume they are two individual lens galaxies, perhaps merging (Jackson et al. 1997; Fassnacht et al. 1999b, in preparation). Long-slit spectroscopy with the Keck telescope along the two galaxies (G1 and G2) shows no sign indicating different redshifts. Another two-lens gravitational lens system (i.e. B1127+385) was recently found by the CLASS collaboration (Koopmans et al. 1999), although it only has two lens images, indicating that gravitational lens systems with multiple lens galaxies are not uncommon. All three HST exposures (F555W, F814W and F160W) of B1608+656 can be found on the Castles web-page (<http://cfa-www.harvard.edu/glensdata/1608.html>) as well.

The relative positions (centroid) of the lens images and lens galaxies were determined in *IRAF*<sup>2</sup> with

---

<sup>2</sup>IRAF (Image Reduction and Analysis Facility) is distributed by the National Astronomy Observatories,

	$x_c$ (")	$y_c$ (")	P.A. (°)	$(b/a)_\Sigma$
G1				
F555W	0.544	-1.060	77→84	≈0.45
F814W	0.521	-1.062	81→77	0.45→0.60
F160W	0.446	-1.063	85→76	–
G2				
F555W	-0.337	-0.976	–	–
F814W	-0.293	-0.965	≈ 75	0.12→0.40
F160W	-0.276	-0.937	–	–

Table 2: Surface brightness distribution parameters of the lens galaxies G1 and G2. The surface brightness centroid is given by  $(x_c, y_c)$ , with an estimated error of 15 mas. The surface brightness position angle (P.A; from north to east) and axis ratio  $((b/a)_\Sigma)$  were determined in *IRAF* by fitting elliptical isophotes as function of radius to the surface brightness distributions of G1 and G2. The range of positions angles (P.A.) and axis ratios from the inner to the outer isophotes is indicated by the arrow. The coordinate system is Cartesian with positive  $x$ -axis pointing west.

respect to the brightest optical image (A). The optical image positions agree with the radio positions to within the observational errors of  $\approx 5$  mas. The lens galaxy positions and their errors are listed in Table 2. The galaxy centroids change as function of wavelength (i.e. between F555W, F814W and F160W), possibly suggesting that G1 and G2 are interacting dynamically (see section 5.3). The galaxy positions are used as additional constraints on the lens mass model.

The surface brightness distributions of G1 and G2 were fitted with elliptical isophotes in *IRAF*. The range of axis ratios and position angles of the elliptical isophotes are listed in Table 2.

## 4. Modeling

### 4.1. The lens mass model

We describe the surface mass distribution of the two lens galaxies with the parameterized elliptical isothermal mass model from Kormann, Schneider & Bartelmann (1994). The surface density distribution of these models is given by

$$\Sigma(\xi_1, \xi_2) = \frac{\sigma^2}{2G} \frac{\sqrt{f}}{\sqrt{\xi^2 + \xi_c^2}}, \quad (1)$$

where  $\xi^2 = \xi_1^2 + f^2 \xi_2^2$ ,  $\sigma$  is a measure of the line-of-sight velocity dispersion,  $\xi_c$  is the lens core radius and  $f = (a/b)_\Sigma$  is the surface density axis ratio. All lengths and positions will from now on be given in arcseconds. The deflection angles and shear components of this mass model are also given in Kormann et al. (1994). It is simple to transform the mass distribution and corresponding deflection and shear fields to any required position and position angle.

We will refer to the (non-)singular isothermal ellipsoidal case as the (NIE) SIE mass distribution. We assume  $\Omega_m = 1$  and  $\Omega_\Lambda = 0$  in a smooth FRW universe, if not specified otherwise. In section 5.4 we discuss non-isothermal mass models.

---

which are operated by the Association of Universities for Research in Astronomy under cooperative agreement with the National Science Foundation.

## 4.2. $\chi^2$ minimization

We use a  $\chi^2$ -minimization procedure to search for the free parameters (mass model parameters, source position and Hubble parameter) that best reproduce the observed image positions, flux density ratios and time delays (Table 1). The  $\chi^2$ -function that is minimized is given by

$$\chi^2 = \sum_{i=1}^4 \left[ \frac{(x_i^o - x_i^m)^2}{\delta x_i^2} + \frac{(y_i^o - y_i^m)^2}{\delta y_i^2} \right] + \sum_{i=1}^4 \left[ \frac{(r_i^o - r_i^m)^2}{\delta r_i^2} \right] + \sum_{i=1}^4 \left[ \frac{(t_i^o - t(h)_i^m)^2}{\delta t_i^2} \right]. \quad (2)$$

The first term on the right-hand side of the equation gives the ‘goodness-of-fit’ between the observed,  $(x, y)_i^o$ , and model,  $(x, y)_i^m$ , image positions, where  $\delta(x, y)_i$  are the  $1\text{-}\sigma$  errors on the observed image positions. The second term gives the goodness-of-fit between the observed,  $r_i^o$ , and model,  $r_i^m$ , flux density ratios. Because the flux density of the lensed object is a free parameter, we normalize the flux density of the brightest observed and model image ( $i = 1$ ) to unity. The third term gives the goodness-of-fit between the observed,  $t_i^o$ , and model,  $t_i^m$ , time delays. The error on the observed time delay is given by  $\delta t_i$ . We normalize the time delay of the leading image to zero. The model time delay is a function of the free parameter  $h = H_0 / (100 \text{ km s}^{-1} \text{ Mpc}^{-1})$ . Thus, minimizing  $\chi^2$  gives not only the mass model parameters and source position, but also a measure of the Hubble parameter,  $H_0$ .

A continuous Simulated Annealing Downhill-Simplex algorithm is used to minimize  $\chi^2$  (Press et al. 1992). Although relatively slow, this method is robust and allows simple adjustment of  $\chi^2$  during the minimization. It also has a high probability of finding the global  $\chi^2$ -minimum compared with faster methods that need the gradients of a complex multi-dimensional  $\chi^2$ -function. The latter is of great importance if we search for the minimum- $\chi^2$  solution in a space of many free parameters ( $\gtrsim 10$ ).

## 5. Results

We investigate several different isothermal and non-isothermal mass models in an attempt to reproduce the observed properties of B1608+656 (Table 1). The two lens galaxies (G1 and G2) are fixed at their observed positions (Table 2). The HST exposures were done using different filters (F555W, F814W and F160W), each giving slightly different galaxy positions. Models with the lens galaxies fixed at the positions

Model	$\sigma$ (km s <sup>-1</sup> )	$(b/a)_\Sigma$	$\theta_{\text{PA}}$ (°)	$r_c$ (")	$\Delta t^{(\text{A-B})}$	$\Delta t^{(\text{C-B})}$	$\Delta t^{(\text{D-B})}$	$H_0^\chi$	$\chi^2$	$\chi^2/\text{NDF}$
F555W-I	253.1, 201.1	0.78, 0.45	63.4, 51.2	0.000, 0.000	18.9 h <sup>-1</sup>	22.5 h <sup>-1</sup>	47.8 h <sup>-1</sup>	62.5	48.1	9.6
F555W-II	253.1, 201.1	0.78, 0.45	63.4, 51.2	0.000, 0.000	18.9 h <sup>-1</sup>	22.5 h <sup>-1</sup>	47.8 h <sup>-1</sup>	62.5	15.6	3.9
F555W-III	248.8, 210.7	0.80, 0.50	61.5, 52.0	0.000, 0.036	18.3 h <sup>-1</sup>	21.8 h <sup>-1</sup>	45.8 h <sup>-1</sup>	60.1	44.2	11.1
F555W-IV	246.9, 214.9	0.81, 0.51	60.6, 52.3	0.000, 0.052	18.0 h <sup>-1</sup>	21.4 h <sup>-1</sup>	44.9 h <sup>-1</sup>	59.0	9.4	3.1
F814W-I	248.2, 207.2	0.88, 0.39	71.9, 53.1	0.000, 0.000	19.2 h <sup>-1</sup>	23.2 h <sup>-1</sup>	45.7 h <sup>-1</sup>	61.6	159.7	31.9
F814W-II	248.2, 207.2	0.88, 0.39	71.9, 53.1	0.000, 0.000	19.2 h <sup>-1</sup>	23.2 h <sup>-1</sup>	45.7 h <sup>-1</sup>	61.6	53.5	13.4
F814W-III	240.1, 223.8	0.93, 0.47	63.0, 54.8	0.000, 0.058	18.2 h <sup>-1</sup>	21.9 h <sup>-1</sup>	42.4 h <sup>-1</sup>	57.7	141.2	35.3
F814W-IV	233.3, 237.2	0.96, 0.52	36.3, 55.9	0.000, 0.105	17.3 h <sup>-1</sup>	20.7 h <sup>-1</sup>	39.4 h <sup>-1</sup>	54.2	22.4	7.5
F160W-I	249.5, 207.1	0.90, 0.31	122.0, 53.8	0.000, 0.000	19.6 h <sup>-1</sup>	24.2 h <sup>-1</sup>	41.0 h <sup>-1</sup>	59.7	622.7	124.5
F160W-II	249.5, 207.1	0.90, 0.31	122.0, 53.8	0.000, 0.000	19.6 h <sup>-1</sup>	24.2 h <sup>-1</sup>	41.0 h <sup>-1</sup>	59.7	172.0	43.0
F160W-III	236.8, 230.8	0.87, 0.42	-25.3, 57.3	0.000, 0.073	18.9 h <sup>-1</sup>	22.9 h <sup>-1</sup>	37.7 h <sup>-1</sup>	57.7	478.9	119.7
F160W-IV	216.8, 266.6	0.70, 0.54	-13.8, 61.1	0.000, 0.183	17.2 h <sup>-1</sup>	20.5 h <sup>-1</sup>	29.2 h <sup>-1</sup>	48.1	19.2	6.4

Table 3: Isothermal mass model parameters of G1 and G2 and determinations of  $H_0$ . Listed are the velocity dispersion ( $\sigma$ ), surface density axis ratio ( $(b/a)_\Sigma$ ), position angle ( $\theta_{\text{PA}}$ ; north to east) and core radius ( $r_c$ ). The first value is for G1, the second for G2. The time delays  $\Delta t$  (in days) are the values determined from the mass model.  $H_0^\chi$  (in km s<sup>-1</sup> Mpc<sup>-1</sup>) was determined through the minimization of  $\chi^2$  as discussed in section 4.2. The last two columns show the minimum- $\chi^2$  and reduced- $\chi^2$  values, respectively. We assume  $\Omega_m = 1$  and  $\Omega_\Lambda = 0$  in this table.

determined from each filter are therefore considered.

It should also be noted that the resulting model flux density ratio of image D ( $r_D$ ) is the only parameter never close to the observed value, throughout all mass models. The magnification depends critically on a combination of second order derivatives of the lens potential and small perturbations can therefore significantly change flux ratios. The delays and positions directly depend on zero-th and first order derivatives of the lens potential, respectively. Hence, they are less sensitive to perturbations by small masses (e.g. Mao & Schneider, 1998). Both the delay and position of image D are in excellent agreement with observations.

For each filter we construct four mass models: (I) SIE+SIE, using all constraints, (II) SIE+SIE, without  $r_D$  as a constraint, (III) SIE+NIE, using all constraints and (IV) SIE+NIE, without  $r_D$  as a constraint. Mass models V and VI, presented in section 5.4, are non-isothermal.

### 5.1. SIE+SIE mass model

The first attempt is to model both G1 and G2 with a SIE mass distribution. In total there are 14 constraints (8 from the image positions, 3 from the flux density ratios and 3 from the time delays) and 9 free parameters (source position, Hubble parameter, velocity dispersions, surface density axis ratios and position angles of G1 and G2). The number of degrees of freedom (NDF) is five. This should give a well constrained set of free parameters, if they are non-degenerate.

Using all constraints, we minimize  $\chi^2$  for the three sets of galaxy positions (Table 2). The resulting model parameters, minimum- $\chi^2$  and Hubble parameters are listed in Table 3 (model I). Using different starting values for the model parameters and a slowly decreasing ‘temperature’ in the Simulated Annealing algorithm (see Press et al. (1992) for a more detailed description of this minimization procedure), we ensure a very high probability of ending up at the global  $\chi^2$ -minimum.

The minimum- $\chi^2$  value is significantly smaller when the HST WFPC2 F555W galaxy positions are used, in comparison with those from the WFPC2-F814W or NICMOS-F160W observations.

The  $\chi^2$ -minimization is repeated, this time without the use of the flux density ratio of image D as a constraint. The resulting model and Hubble parameters (Table 3; models II) are similar to models I, but  $\chi^2$  has decreased more than expected on the basis of the decreased number of degrees of freedom (NDF=4). The flux density ratio of image D contributes disproportionately to  $\chi^2$  compared with the other constraints,

possibly due to a local perturbation of the lens potential (e.g. milli- or micro-lensing).

Lens model F555W-II has the smallest  $\chi^2$  value of all SIE+SIE mass models in Table 3. Figure 1 (left) shows both the critical-curve and caustic structure of this model and its time-delay surface. When moving a source from outside the caustic structure – e.g. where the source is singly imaged – the number of lens images changes by two, each time a caustic is crossed. We therefore expect the SIE+SIE models to show seven images, of which two are highly de-magnified, because they are located near the surface density singularities of G1 and G2.

However, the fifth image should be visible. It is formed on the saddle point of the time-delay surface near galaxy G2 (Fig. 1). Its magnification is around 0.2. This should make it visible ( $\gtrsim 50\text{-}\sigma$  detection) in the deep VLA A-array observations available to us (Paper I). The image, however, is not detected, which poses a strong restriction on the allowed set of models.

## 5.2. SIE+NIE mass model

The primary reason to introduce a small core radius for G2 is to remove the fifth image formed at the saddle-point of the time-delay surface between G1 and G2 (Fig. 1). If the core radius is large enough, there are no extrema on the time-delay surface and thus no images will form between G1 and G2 (e.g. Schneider et al. 1992).

We minimize  $\chi^2$  again for the three sets of galaxy positions. The core radius of G2 is left free (NDF=4; models III). We repeat this without  $r_D$  as a constraint (NDF=3; models IV). The resulting model parameters and Hubble parameters are listed in Table 3. Lens model F555W-IV is shown in Fig.1 (right). The recovered image positions, flux density ratios and time delays from model F555W-IV are listed in Table 5.

A significant improvement in the reduced  $\chi^2$  is obtained with models IV over models II (no core radius for G2) and models I and III (with  $r_D$  as constraint). There is also a decrease in the reduced  $\chi^2$  from models F160W-IV to F555W-IV. This suggests that the mass centers of G1 and G2 are more closely associated with the emission centroids from the HST F555W exposure.

The source now only crosses two caustics, when moving it from outside the caustic structure to its model position shown in Fig.1 (right). Thus five images instead of seven are formed. This solves the ‘central-image’ problem, even though no lower limit on the core radius of G2 was imposed. One of

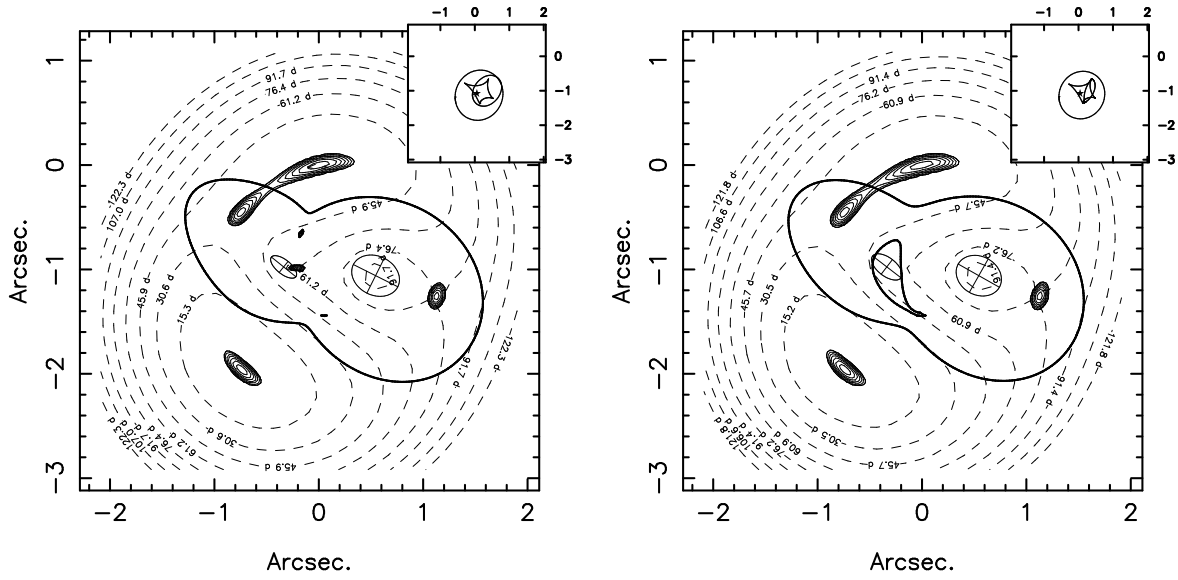


Fig. 1.— Left: Time-delay surface (dashed lines), critical curves (thick lines) and caustic structure (sub-panel) of the SIE+SIE lens model F555W-II. The lens images are the projections onto the image plane of a Gaussian shaped source (star) with a FWHM of 0.1 arcsec. The cross-haired ellipses indicate the position, axis-ratio and position angle of G1 and G2. Right: Idem, but for the SIE+NIE mass model F555W-IV.

the five images forms near the surface density singularity of G1 and is highly de-magnified, because the magnification is almost inversely proportional to the surface density close to the singularity (Kormann, Schneider & Bartelmann 1994). Only four observable lens images remain, as is required by the observational constraints.

### 5.3. Models with constrained position angles

Comparing the mass model position angles of G1 and G2 (Table 3), with the observed surface brightness position angles (Table 2), we see a systematic  $\approx 20$  degree difference.

We attempted several models with position angles for G1 and G2 in the range indicated in Table 2. The lens galaxy positions were not constrained and they were allowed to have a finite core radius. Even though the system is close to being under-constrained, no satisfactory solutions with position angles close to those listed in Table 2 could be obtained (i.e.  $\chi^2 \gg 10^6$ ).

The  $\approx 20$  degree difference in position angle between surface brightness and surface density of G1 and G2 therefore remains. There are several possible solutions: (i) The lens galaxies (G1 and G2) have tri-axial halos, producing a misalignment between surface brightness and the projected surface density of the dark matter halo (Keeton, Kochanek, & Seljak 1997). (ii) A dynamical interaction between G1 and G2 could introduce a physical misalignment between the halo and the luminous matter. A ‘merger’ scenario could explain why G1 and G2 look like post-starburst galaxies (Myers et al. 1995) and have much bluer colors than expected for ellipticals (Keeton, Kochanek, & Falco 1998; Fassnacht et al. 1999b, in preparation). Star-formation associated with the deepest part of the lens potential would also explain why the galaxy positions from the HST F555W exposure seem most closely associated with the lens mass centers, although extinction by dust could make this argument more complicated. (iii) External mass components can create the presence of an external shear near G1 and G2, which introduces an apparent misalignment of surface brightness and density position angles (Keeton, et al. 1997). B1608+656 is part of a small group of galaxies (Fassnacht et al. 1999b, in preparation). However, based on their luminosities, these galaxies do not seem massive enough to cause significant perturbations of the lens potential. Moreover, we have added an external shear to our best isothermal mass model (F555W-IV; Table 3) and find no decrease in  $\chi^2$ , even though NDF decreases by two. (iv) The group of galaxies (including G1 and G2) is associated with inter-galactic gas. This is often seen in Hickson compact groups (Hickson 1982) through X-ray emission (e.g. Pildis, Bregman & Evrard 1995). Although the group of galaxies associated with B1608+656 is not

very compact or massive, some gas could still be associated with it. If this gas ‘halo’ is misaligned with G1 and G2, the inferred surface density position angles can deviate from the surface brightness position angles, if the gas is not accounted for in the mass model.

In the cases (iii) and (iv), it remains peculiar that all image positions, time delays and two out of the three flux density ratios are reconstructed relatively well by the best mass model (F555W-IV). This is hard to understand if a large-scale mass component or external shear is missing from the mass model. We therefore prefer either a tri-axial halo for G1 and G2 or a misalignment of the halo and the luminous matter due to dynamical interactions of G1 and G2. Both can explain the misalignment in position angle without invoking new mass components.

#### 5.4. Non-isothermal mass models

To investigate the validity of using an isothermal mass distribution, we also tested models with surface density profiles given by

$$\Sigma(\xi_1, \xi_2) = \frac{\Sigma_0}{\left[1 + \left(\frac{\xi^2}{\xi_c^2}\right)\right]^{-\gamma}}. \quad (3)$$

The normalization of  $\Sigma_0$  is chosen to agree with that of eqn. (1) for  $\gamma = 1/2$  (the isothermal model). The mass inside some arbitrary radius diverges for profiles with  $\gamma > 1/2$  and  $\xi_c = 0$ . We therefore place a lower limit of  $10^{-3}$  arcsec on the core radii of both G1 and G2. Both galaxies are placed on the observed F555W galaxy positions, which seem to best represent their mass centers (section 5.1). We use the code developed by Barkana (1998) to calculate the deflection angle and magnification for models with  $\gamma \neq 1/2$ .

##### 5.4.1. Constraints on the radial mass profile

Using all observational constraints, we minimize  $\chi^2$  as described in sections 5.1–3 (model F555W-VI). The mass distributions of G1 and G2 are given the same value of  $\gamma$ . We repeat this without flux ratio  $r_D$  as a constraint (model F555W-V). The model parameters, Hubble parameters and minimum- $\chi^2$  values are listed in Table 4.

The table shows that  $\chi^2$  minimizes in the range  $\gamma \approx 0.4$ – $0.6$ , taking both models F555W-V and F555W-VI into account. The use of  $r_D$  as constraint (model F555W-VI) increases the  $\chi^2$  values by a factor of about 10. If we assume that  $r_D$  is correct and one of the other three images has an incorrect flux density

Model	$\gamma$	$\sigma$ (km s <sup>-1</sup> )	$(b/a)_\Sigma$	$\theta_{\text{PA}}$ (°)	$r_c$ (")	$H_0^\chi$	$\chi^2$
F555W-V	0.3	293.2, 220.7	0.91, 0.67	-10.8, 56.5	0.152, 0.017	27.4	5.8
	0.4	274.5, 210.9	0.96, 0.57	36.1, 53.2	0.095, 0.001	41.8	1.4
	0.5	269.6, 214.4	0.91, 0.53	54.7, 52.0	0.148, 0.078	50.5	4.6
	0.6	271.0, 222.4	0.90, 0.51	55.2, 51.6	0.231, 0.150	54.7	7.2
	0.8	294.1, 230.1	0.92, 0.48	49.3, 50.6	0.462, 0.249	56.0	12.3
	1.0	304.1, 243.2	0.93, 0.48	41.9, 50.5	0.599, 0.344	57.4	19.8
F555W-VI	0.3	270.0, 229.4	0.92, 0.68	-5.4, 56.7	0.003, 0.001	29.9	195.6
	0.4	261.4, 216.1	0.94, 0.58	45.4, 53.6	0.007, 0.005	44.1	98.0
	0.5	250.6, 207.1	0.80, 0.48	62.3, 51.7	0.001, 0.022	60.9	45.2
	0.6	237.0, 209.8	0.65, 0.44	64.3, 51.4	0.018, 0.075	74.8	37.0
	0.8	237.8, 211.2	0.55, 0.36	66.0, 50.5	0.118, 0.150	89.9	66.5
	1.0	239.5, 216.3	0.50, 0.33	66.7, 50.2	0.191, 0.211	98.5	105.8

Table 4: Mass model parameters of G1 and G2 for different mass profiles and determinations of  $H_0$ . Listed are the profile parameter  $\gamma$ , velocity dispersion ( $\sigma$ ), surface density axis ratio ( $(b/a)_\Sigma$ ), position angle ( $\theta_{\text{PA}}$ ; north to east) and core radius ( $r_c$ ). The first value is for G1, the second for G2. The Hubble parameter  $H_0$  (in km s<sup>-1</sup> Mpc<sup>-1</sup>) was determined through the minimization of  $\chi^2$  (section 4.2). The last column shows the minimum- $\chi^2$  value. We assume  $\Omega_m = 1$  and  $\Omega_\Lambda = 0$  in this table.

ratio, we still find a comparable increase in  $\chi^2$ . So for all models in this range of mass profiles,  $r_D$  is the only observable that can not be reasonably matched to its model value. The inclusion of  $r_D$  as a constraint changes  $\gamma$  of the best model from about 0.4 to 0.6. The lowest values of  $r_D$  that we find is 0.24 for model F555W-VI with  $\gamma = 0.6$ . Thus, keeping in mind that  $r_D$  could be larger than 0.17 – preferred by all models (independent of  $\gamma$ ) – the value of  $\gamma = 0.6$  can be overestimated.

When  $\gamma < 0.5$ , the position angle of G1 rapidly decreases until a prolate halo is preferred with  $\theta_{\text{PA,G1}} \approx -(5 - 11)$  degrees for  $\gamma = 0.3$ . Values of  $\gamma$  much smaller than 0.5 are therefore on the basis of comparison with the surface brightness positions angle not very likely. Moreover, for  $\gamma \leq 0.4$  all minimum- $\chi^2$  models form a fifth central image, similar to the SIE+SIE models (section 5.1). This is not the case for  $\gamma \geq 0.5$ .

The range of  $\gamma \approx 0.4-0.6$  for G1 and G2 agrees with constraints on  $\gamma$  from the gravitational lenses Q0957+561 (Grogin & Narayan 1996a; Barkana et al. 1998) and MG1654+1346 (Kochanek 1995). The models for both of these prefer values close to  $\gamma=0.5$  (i.e. isothermal).

#### 5.4.2. The radial mass profile and $H_0$

In Figure 2, we plot  $H_0$  versus  $\gamma$ . For models F555W-V,  $H_0$  increases from 27 to 57  $\text{km s}^{-1} \text{Mpc}^{-1}$  between  $\gamma = 0.3$  and 1.0. For models F555W-VI,  $H_0$  increases from about 30 to 99  $\text{km s}^{-1} \text{Mpc}^{-1}$ .

Because models F555W-V are not constrained by  $r_D$ , the core radius of G1 can rapidly increase with  $\gamma$  (Table 4). This gives an overall flatter mass profile of G1 inside the Einstein radius compared with larger radii ( $\gg \xi_c$ ), reducing the growth of  $H_0$  for  $\gamma > 0.5$ . However, larger core radii of G1 also give values for  $r_D \gtrsim 0.5$ , which is outside any reasonable range. In models F555W-VI the growth of  $\xi_c$  is suppressed by the small value of  $r_D$ .

Not only do B1608+656 and Q0957+561 have similar mass profiles, they also give similar values of  $H_0$  as we will see later on. In the rest of the paper we assume that both G1 and G2 are isothermal. The value of  $\gamma$  is conservatively taken as  $0.50 \pm 0.10$  for the reasons given in section 5.4.1. The models for  $\gamma = 0.3, 0.5$  and 1.0 (Table 4) are shown in Figure 3.

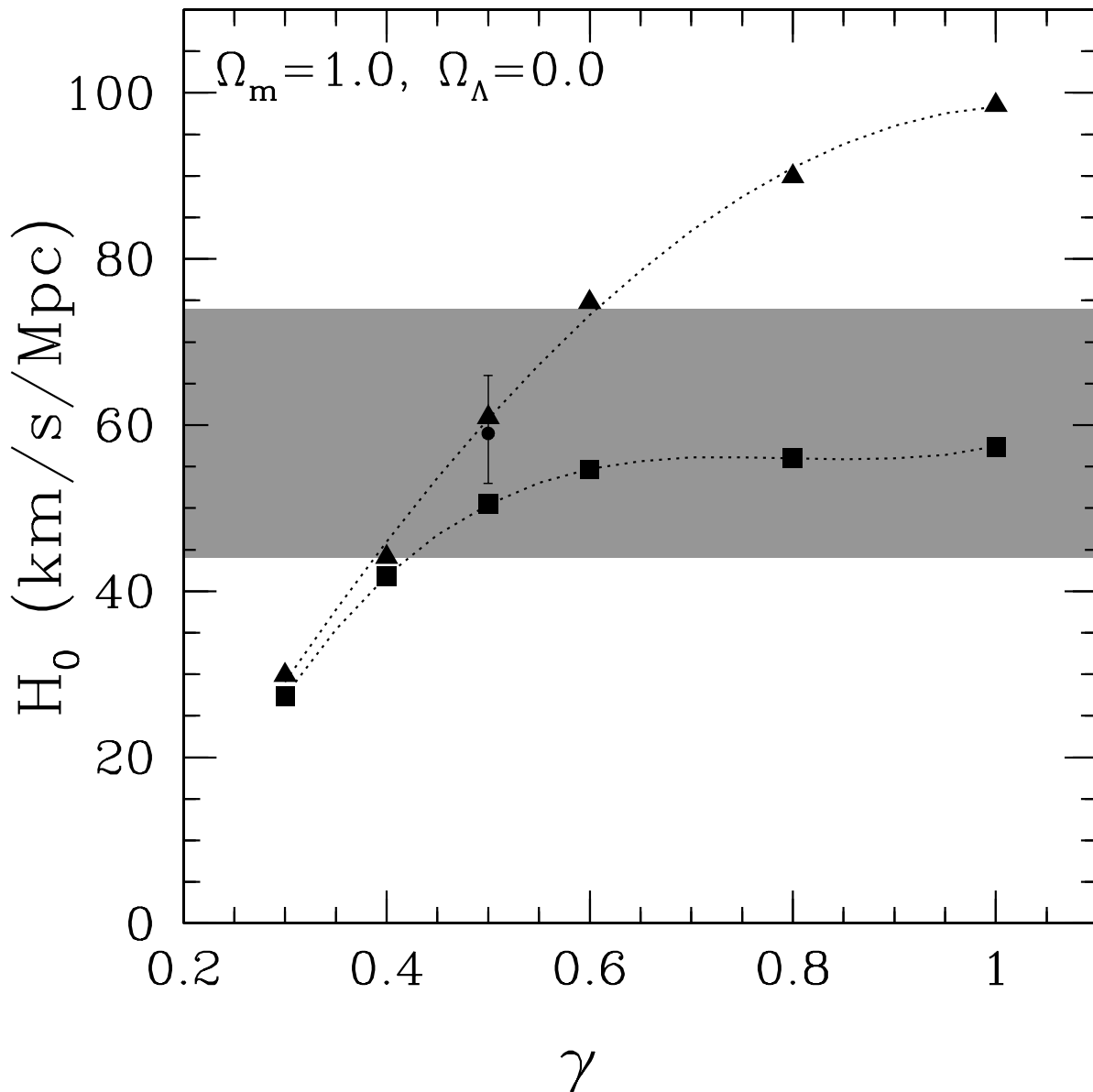


Fig. 2.— The Hubble parameter  $H_0$  from B1608+656 plotted against the profile parameter  $\gamma$  for the minimum- $\chi^2$  mass model. The triangles indicate the optimum value of  $H_0$  obtained from the  $\chi^2$  minimization with all flux density ratios as constraints. The squares indicate the optimum value of  $H_0$  when omitting the flux density ratio of image D. The shaded region indicates the range of  $H_0$  when  $\gamma = 0.50 \pm 0.10$  (section 5.4.1). This introduces a systematic error of  $\pm 15 \text{ km s}^{-1} \text{ Mpc}^{-1}$ . The filled dot and the  $2\text{-}\sigma$  statistical error bars at  $\gamma = 0.5$  indicate the value of  $H_0$  from the ‘best’ isothermal mass model (F555W-IV; Table 3; section 6). The dotted lines are a third-order polynomial fit.

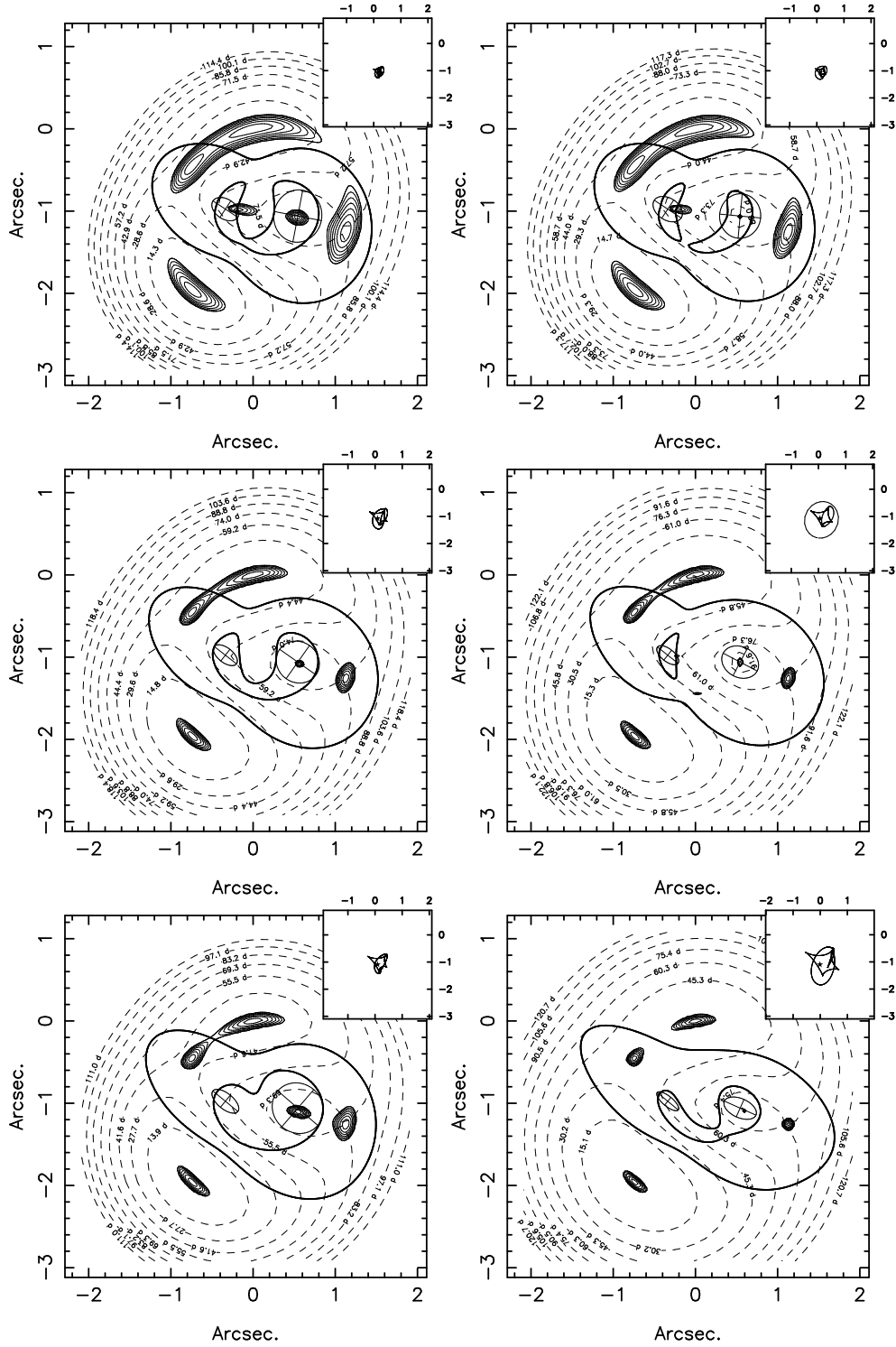


Fig. 3.— Same as Fig. 1, now for models F555W-V and F555W-VI. The figures on the left (upper to lower) show models F555W-V for  $\gamma = 0.3, 0.5$  and  $1.0$ , respectively. The figures on the right are for models F555W-VI.

## 6. The Hubble parameter from B1608+656

The best estimate of the Hubble parameter (i.e.  $H_0^x$ ) from B1608+656 ranges from 60 to 63  $\text{km s}^{-1} \text{Mpc}^{-1}$  for the SIE+SIE mass models. This range increases to 48 – 60  $\text{km s}^{-1} \text{Mpc}^{-1}$  for the SIE+NIE mass models (Table 3). All values of  $H_0$  are given for a flat universe with  $\Omega_m=1$ , if not specified otherwise.

If we only consider models with (i) relatively low reduced  $\chi^2$  values ( $\lesssim 10$ ) and (ii) models that do not give a fifth observable image, then only models IV (Table 3) remain viable candidates. The best isothermal model, F555W-IV, gives  $H_0^x = 59 \text{ km s}^{-1} \text{Mpc}^{-1}$  and a very smaller scatter ( $\approx 1\%$ ) between the values of  $H_0$  from the individual time delays. This small scatter is a coincidence and not a result from the  $\chi^2$ -minimization. We have tried different values for the delays, which gave proportionally different values of  $H_0$ . Even without these additional three constraints, model F555W-IV remains the best model (i.e. smallest  $\chi^2$ ).

We will therefore take  $H_0 = 59 \text{ km s}^{-1} \text{Mpc}^{-1}$  to be our best estimate of the Hubble parameter from B1608+656, given that G1 and G2 can be modeled with an isothermal mass distribution. Model F555W-IV reproduces all observables within an acceptable range, except for the flux density ratio of image D. It does not produce a bright central image as required by its absence in the observations. It is the only plausible isothermal model that cannot be excluded at very high confidence level, based on its  $\chi^2$  (assuming the flux density ratio of image D is indeed perturbed). The surface density position angles of G1 and G2 are also within an acceptable range from the surface brightness position angles, considering that G1 and G2 could be merging (Jackson et al. 1997; Fassnacht et al. 1999b, in preparation). All other models in Table 3 can be rejected on the basis of one of these criteria.

Clearly, an uncertainty remains regarding the explicit assumption of the isothermal mass distribution for G1 and G2. This is reflected in the systematic error on  $H_0$ , given in section 6.1. However, the use of similar isothermal mass models makes a direct comparison with other lens systems possible, if their radial mass profile is ill-constrained (Schechter 1998; section 7).

### 6.1. The errors on $H_0$ from B1608+656

To estimate the statistical error on  $H_0$  found from model F555W-IV, we vary it over a range of fixed values and minimize  $\chi^2$ . We determine the range within which the minimum- $\chi^2$  value increases by less than

4.0. This range indicates the 95.4% or  $2\text{-}\sigma$  (statistical) confidence range of  $H_0$  (Press et al. 1992). We find:

$$H_0^{1608} = 59_{-6}^{+7} \text{ km s}^{-1} \text{ Mpc}^{-1} \quad (\Omega_m = 1, \Omega_\Lambda = 0).$$

We regard this as the ‘best’ estimate of  $H_0$  determined from the available observational constraints of B1608+656, under the explicit assumptions mentioned previously.

The  $\approx 0.1$  error on  $\gamma$  introduces a systematic error in  $H_0$  of  $\pm 15 \text{ km s}^{-1} \text{ Mpc}^{-1}$  (see Fig.2). This error incorporates the much smaller uncertainties on  $H_0$  as a result of the chosen galaxy positions, core radii or sets of constraints (Tables 3 and 4).

## 7. $H_0$ from other gravitational lens systems

Four other gravitational lens systems have yielded values for  $H_0$  at present. We will discuss them separately and compare the results with those from B1608+656. All values of  $H_0$  are given for a flat universe with  $\Omega_m=1$ , if not specified otherwise.

(i) The first discovered gravitational lens system Q0957+561 (Walsh et al. 1979) recently yielded  $H_0 = 63 \pm 12 \text{ km s}^{-1} \text{ Mpc}^{-1}$  (95% confidence) from a time delay of  $417 \pm 3$  days (95% confidence) found from optical light curves (Kundić et al. 1997b). Although less constrained, Haarsma et al. (1999) found a delay consistent with this from radio light curves. The error on  $H_0$  is dominated by uncertainties in the model of the mass distribution of the lens (Kundić et al. 1997b). Barkana et al. (1998) showed that the error on  $H_0$  could be somewhat larger than found by Kundić et al. (1997b), due to increased uncertainties in the assumed mass model. Moreover, a new determination of the velocity dispersion of the cluster lens by Tonry & Franx (1999) indicates  $H_0=70 \pm 7$  or  $72 \pm 7 \text{ km s}^{-1} \text{ Mpc}^{-1}$  ( $1\text{-}\sigma$ ), using the SPLS or FGS models from Grogin & Narayan (1996a, 1996b), respectively. The surface density profile of the dominant lens mass distribution in Q0957+561 was shown to be close to isothermal (Grogin & Narayan 1996a; Barkana et al. 1998).

(ii) The second gravitational lens system discovered, PG1115+080 (Weymann et al. 1980), recently gave a value of  $H_0 = 44 \pm 4 \text{ km s}^{-1} \text{ Mpc}^{-1}$  ( $1\text{-}\sigma$ ) using an isothermal mass model (Impey et al. 1997) and the time delays found by Schechter et al. (1997). This value is low compared with most determinations of  $H_0$ , not only those from gravitational lensing. The lens mass consists of an elliptical galaxy and a nearby galaxy group. For truncated halo models or constant M/L-ratio models,  $H_0$  could go up to as much as  $65 \pm 5 \text{ km s}^{-1} \text{ Mpc}^{-1}$ . However, the large B-band M/L-ratios ( $\geq 13$ ) suggests that dark matter is present. This makes

constant M/L models unlikely, if the luminous and dark matter distributions are different (Impey et al. 1997). For  $H_0$  to be  $\gtrsim 60 \text{ km s}^{-1} \text{ Mpc}^{-1}$ , the dark matter halo has to be truncated just outside the Einstein radius. This suggests that the lens is almost completely stripped of its halo, possibly by interaction with the nearby compact group (Kundić et al. 1997a; Tonry 1998; Impey et al. 1997). PG1115+080 remains a complicated system with large uncertainties, mostly due to the uncertain contribution of the surface density of the group at the position of the primary lens galaxy. The lack of strong radio emission from the lens images limits the information that can be obtained on the mass distribution through deep radio or VLBI observations (e.g. Q0957+561). However, the lensed quasar forms an optical Einstein ring around the lens, providing valuable additional information about the lens potential.

(iii) Recently, a robust time delay of  $10.5 \pm 0.4$  days (95% confidence) was determined between the two compact radio images in the radio Einstein ring B0218+357 (Biggs et al. 1999). Preliminary modeling based on the VLBI structure in both images (Patnaik et al. 1995) yielded  $H_0 = 69_{-19}^{+13} \text{ km s}^{-1} \text{ Mpc}^{-1}$  (95% confidence), using an isothermal mass model (Biggs et al. 1999). B0218+357 is an ‘isolated’ spiral galaxy lens and has no apparent nearby massive companions.

(iv) The gravitational lens PKS1830-211 consists of an extended source lensed into an Einstein ring (e.g. Jauncey et al. 1991). The bright compact core of the flat-spectrum source is lensed in two images embedded in the ring structure. The source is highly variable (e.g. Lovell et al. 1998) and can therefore be used to determine the time delay between the two images. Van Ommen et al. (1995) found a time delay of  $44 \pm 9$  days, derived from very poorly sampled light curves. However, recently an unambiguous delay of  $26_{-5}^{+4}$  days was found by Lovell et al. (1998). With the mass model from Nair et al. (1993) and the recently determined source redshift  $z_s = 2.507 \pm 0.002$  (Lidman et al. 1998; private communication), this delay yields  $H_0 = 65_{-9}^{+16} \text{ km s}^{-1} \text{ Mpc}^{-1}$  ( $1-\sigma$ ) (Lovell et al. 1998). To be able to compare the determination of  $H_0$  from PKS1830-211 with those from the other four gravitational lens systems, we model the lens galaxy as a singular isothermal mass distribution (Kormann, Schneider & Bartelmann 1994). We place the mass distribution at the galaxy position determined by Nair et al. (1993) and minimize the difference between the observed and model image positions and flux density ratio. We then find  $H_0 = 75_{-10}^{+18} \text{ km s}^{-1} \text{ Mpc}^{-1}$  ( $1-\sigma$ ). We will use this value in the rest of the paper.

**7.1. The average of  $H_0$  from B0218+357, Q0957+561, PG1115+080, B1608+656 and PKS1830-211**

There is excellent agreement between  $H_0$  from B0218+357, Q0957+561, B1608+656 and PKS1830-211 (from now on called sample  $\mathcal{L}$ ; see Fig. 4). The rms scatter in  $H_0$  from these four systems is  $\approx 10\%$ , comparable to the  $1-\sigma$  statistical error on  $H_0$  from the individual gravitational lens systems. This strongly suggests that (i) systematic effects between these four systems are relatively small and (ii) some systematic effect remains in PG1115+080. Is this small number statistics or are the quoted systematic errors on  $H_0$  overestimated? If the systematic errors were not correlated between the different lens systems, a scatter of some 20 per cent could be expected.

The common factor between *all* five gravitational lens systems, however, is the use of the elliptical isothermal mass model. The systematic error on  $H_0$  is dominated by deviations from this mass profile. The rms scatter in  $H_0$  therefore suggests that a ‘universal’ mass profile can reasonably well describe the spiral galaxies in B0218+357 and PKS1830-211, the two (elliptical) galaxies in B1608+656 and the cluster elliptical in Q0957+561. Moreover, both B1608+656 and Q0957+561 suggest that this profile is close to isothermal (section 5.4.1).

Extra constraints on the radial mass profile will therefore have the largest impact on the reliability of  $H_0$  from these lenses. In B0218+357 and PKS1830-211, constraints on the radial mass profile can be obtained through a detailed analysis of the radio Einstein ring (e.g. Kochanek & Narayan 1992; Biggs et al. 1999), in B1608+656 through analysis of the optical arcs and in Q0957+561 through observations of additional sources in the field and new radio structure (e.g. Barkana et al. 1998). Also in PG1115+080, observations of the optical Einstein ring could provide valuable new information on the lens potential (e.g. Impey et al. 1998).

Thus, under the explicit assumption that the mass models are isothermal, the errors on  $H_0$  appear dominated by statistical errors. We therefore take the average of  $H_0$  (with equal weights) from sample  $\mathcal{L}$ . We find

$$H_0^{\text{GL}} = 69 \pm 7 \text{ km s}^{-1} \text{ Mpc}^{-1} \quad (\Omega_m = 1, \Omega_\Lambda = 0),$$

where the error is the  $2-\sigma$  error on the average (i.e not the scatter). We have used the latest determination of  $H_0$  from Q0957+561 by Tonry & Franx (1999). If we add PG1115+080 to the  $\mathcal{L}$  sample, this value decreases to  $64 \pm 11 \text{ km s}^{-1} \text{ Mpc}^{-1}$  ( $2-\sigma$ ).

The  $\mathcal{L}$  sample of gravitational lens systems gives  $H_0$  within 10% accuracy at a  $2\text{-}\sigma$  confidence level. It also excludes the value from PG1115+080 with  $\gtrsim 4\text{-}\sigma$  (see section 8 and Table 6). However, the systematic errors on this value of  $H_0$  remain around 20 per cent and it is crucial to reduce this through additional observations, which can pin down their precise radial mass profiles.

### 8. A comparison between Gravitational lens, SNIa, S-Z and local determinations of $H_0$

To determine  $H_0$  on cosmological scales one can also make use of Type Ia Supernovae or the Sunyaev-Zel'dovich (SZ) effect.

In principle the S-Z effect is very powerful method to determine  $H_0$ , but systematic effects, such as cluster elongation and clumpiness, are poorly understood. Most measurements give relatively low values of  $H_0$ . However, X-ray selection minimizes the effects of cluster elongation. From a sample of X-ray selected clusters Myers et al. (1997) recently found  $H_0=54\pm 14 \text{ km s}^{-1} \text{ Mpc}^{-1}$  ( $1\text{-}\sigma$ ).

The best determination of  $H_0$  from Type-Ia Supernovae comes from the High-Z Supernovae Search Team (Riess et al. 1998). Based on 50 SNe-Ia events, they find  $H_0^{\text{SNIa}} = 65 \pm 7 \text{ km s}^{-1} \text{ Mpc}^{-1}$  ( $1\text{-}\sigma$ ; independent of  $\Omega_m$  and  $\Omega_\Lambda$ ). The error includes uncertainties on the calibration of the SNIa absolute magnitudes and the zeropoint of the Cepheid distance scale (e.g. Riess et al. 1998). Their results also seem to (i) rule out  $\Omega_m = 1$  for a flat universe at  $\gtrsim 7\text{-}\sigma$  confidence and (ii) indicate  $\Omega_\Lambda > 0$  at  $\gtrsim 3\text{-}\sigma$  confidence (e.g. Riess et al. 1998). However, the determination of  $H_0$  from SNe Ia is a ‘standard-candle’ method. It can be influenced by a host of systematic effects, such as evolution, extinction, selection biases and weak lensing (Riess et al. 1998). Moreover, the determination depends on the Cepheid distance scale and is therefore not independent of the local determinations. This value should therefore be regarded with some caution.

So far, we have only regarded  $H_0$  from gravitational lenses in a flat universe with  $\Omega_m=1$ . But evidence has been mounting over the last few years supporting a low density universe with  $\Omega_m=0.2\text{-}0.3$  (e.g. Carlberg et al. 1996; Bahcall, Fan & Cen 1997; Riess et al. 1998).

In a low-density universe with  $\Omega_m=0.3$  and  $\Omega_\Lambda$  ranging from 0.0 to 0.7, the Hubble parameter determined from gravitational lenses increases by about 7%, depending on the precise lens and source redshifts. We then find

$$H_0^{1608} = (65 - 63)_{-6}^{+7} \text{ km s}^{-1} \text{ Mpc}^{-1}$$

Image	A	B	C	D
$x_i^m$ (")	0.0000	-0.7380	-0.7446	+1.1284
$y_i^m$ (")	0.0000	-1.9612	-0.4537	-1.2565
$r_i^m$	$\equiv 1.00$	0.55	0.51	0.29
$\mu_i$	6.09	3.36	-3.11	-1.78
$t_i^m$ (d)	$18.0 h^{-1}$	0.0	$21.4 h^{-1}$	$44.9 h^{-1}$

Table 5: Image properties as determined from our best model (F555W-IV; Table 3). Except for  $r_D$  all observables are well recovered (see Table 1). The best estimate of  $h$  is 0.590 from model F555W-IV. The image magnification and parity is given by  $\mu_i$ . The source position is (0.0459", -1.0774").

Method	$\Omega_m$	$\Omega_\Lambda$	$H_0$
1	1.0	0.0	$64 \pm 11$
1	0.3	0.0–0.7	$68 \pm 13$
2	1.0	0.0	$69 \pm 7$
2	0.3	0.0–0.7	$74 \pm 8$
3	1.0	0.0	$64 \pm 7$
3	0.3	0.0–0.7	$67 \pm 9$
4	1.0	0.0	$67 \pm 6$
4	0.3	0.0–0.7	$70 \pm 7$

Table 6: The average of  $H_0$  from local and cosmological determinations. The error indicates the  $2\text{-}\sigma$  error on the averages. The methods are: (1) All lenses (i.e. B0218+357, Q0957+561, PG1115+080, B1608+656 and PKS1830-211), (2) all lenses, except for PG1115+080, (3) all methods (i.e. all lenses, SNe Ia, S-Z and local) and (4) all methods, except for PG1115+080.

for  $\Omega_m=0.3$  and  $\Omega_\Lambda=0.0-0.7$ , with  $2\text{-}\sigma$  errors. The average from sample  $\mathcal{L}$  becomes

$$H_0^{\text{GL}} = 74 \pm 8 \text{ km s}^{-1} \text{ Mpc}^{-1} \quad (\Omega_m = 0.3, \Omega_\Lambda = 0.0 - 0.7),$$

with  $2\text{-}\sigma$  errors (including the range in  $\Omega_\Lambda$ ). If we add PG1115+080 to the  $\mathcal{L}$  sample, this value decreases to  $68 \pm 13 \text{ km s}^{-1} \text{ Mpc}^{-1}$ . For a low density universe with  $\Omega_m = 0.3$ , a robust value of  $H_0^{\text{GL}}$  is found which only weakly depends on  $\Omega_\Lambda$  ( $\lesssim 2\%$ ). It is also in good agreement with the determination from Type Ia Supernovae.

Moreover, the cosmological gravitational lens determination of  $H_0$  agrees best with the local determination of  $H_0 = 73 \pm 6$  (statistical)  $\pm 11$  (systematic)  $\text{km s}^{-1} \text{ Mpc}^{-1}$  (*Hubble Space Telescope* Key Project for the Extra-galactic distance Scale; Freedman et al. 1998) in a low density universe. Once both the local and gravitational lens determinations of  $H_0$  are well constrained (i.e. small statistical and systematic errors), the agreement between both values can be used to constrain the density of the universe and possibly the cosmological constant (e.g. Refsdal 1966; Kayser & Refsdal 1983). However, if the local determinations of  $H_0$  are systematically larger than the determinations on cosmological scales, this could suggest that we live in an under-dense part of the universe (e.g. Zehavi et al. 1998).

We have plotted the local determination of  $H_0$  from Freedman et al. (1998) and those determined on cosmological scales in Figure 4. It shows that all determinations of  $H_0$  agree with those from sample  $\mathcal{L}$  to within  $1\text{-}\sigma$ , except for PG1115+080. To be complete, we have listed the averages of  $H_0$  from different combinations of methods and cosmologies in Table 6. It shows a maximum of  $10 \text{ km s}^{-1} \text{ Mpc}^{-1}$  difference between several determinations of the average of  $H_0$ . We have included the determination of  $H_0$  from PG1115+080 in methods 1 and 3 (see Table 6), although it lies  $\gtrsim 4\text{-}\sigma$  outside any range listed in Table 6. The probability of having one  $4\text{-}\sigma$  outliers in a sample of five is  $\ll 1\%$ , making it unlikely that this value is due to a statistical fluke only.

The agreement on  $H_0$  from four out of five gravitational lens systems, the SNIa, the S-Z and local determinations is also an independent confirmation that the lens mass models should not deviate too much from isothermal, as was already shown from some of the individual gravitational lens systems. If we combine the strong dependence on  $\gamma$  of  $H_0$  from B1608+656 (Fig.2) with the demand that  $H_0^{\text{GL}}$  should be between the local and SNIa determinations, then on average  $\gamma$  for the  $\mathcal{L}$  sample should not deviate by more than about 10 per cent from  $\gamma=0.50$  (isothermal) for  $\Omega_m = 0.3$  and  $\Omega_\Lambda = 0.0-0.7$ .

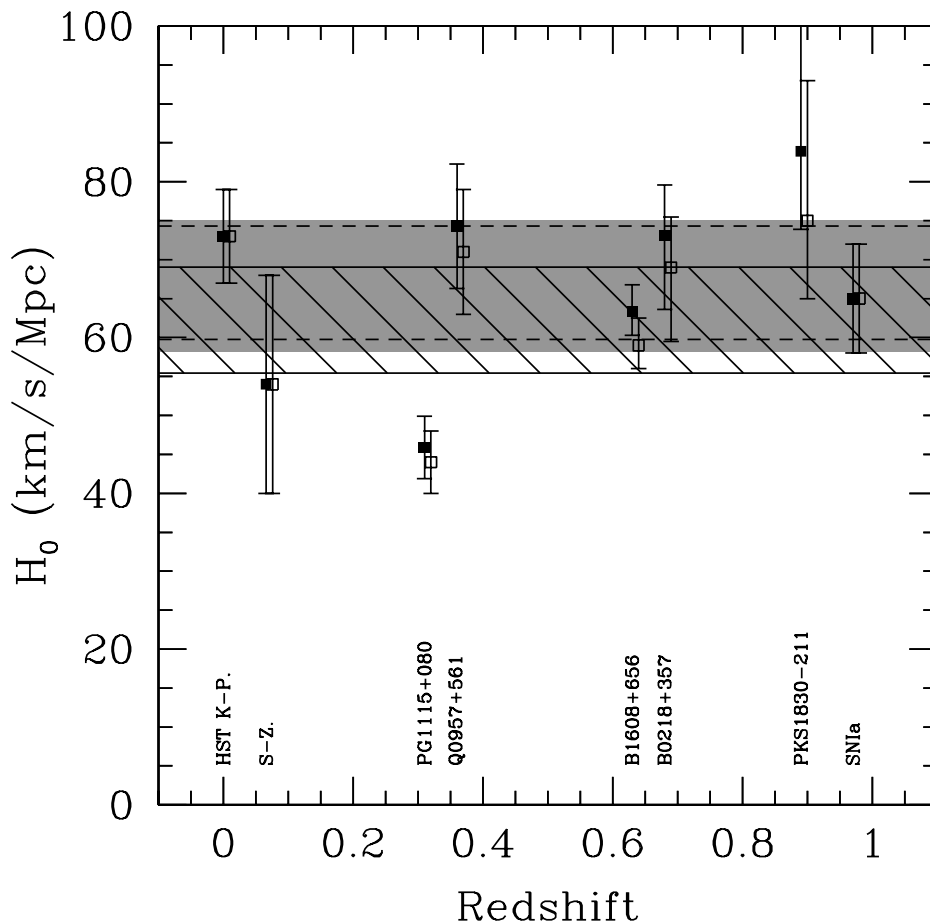


Fig. 4.— The Hubble parameter determined on cosmological scales plotted as function of redshift. The average local value, presented by Freedman et al. (1998; HST Key Project for the Extragalactic Distance Scale) has a redshift  $z = 0$ . The SNIa determination has been placed on the highest redshift SNIa in the sample (Riess et al. 1998). The redshift for the S-Z determination of  $H_0$  is the average cluster redshift in the sample (Myers et al. 1997). The gravitational lenses have been placed at the primary lens redshift. The open symbols are the values of  $H_0$  for  $\Omega_m = 1$  and  $\Omega_\Lambda = 0$ , the closed symbols for  $\Omega_m = 0.3$  and  $\Omega_\Lambda = 0.7$ . The local, S-Z and SNIa determinations are almost independent of  $\Omega_m$  and  $\Omega_\Lambda$ . The densely shaded region indicates the  $\pm 2\text{-}\sigma$  region around the average of  $H_0$  determined from the  $\mathcal{L}$  lens sample for  $\Omega_m = 0.3$  and  $\Omega_\Lambda = 0.7$ . The dashed horizontal lines indicate the  $\pm 2\text{-}\sigma$  region around the average of  $H_0$  determined from the  $\mathcal{L}$  lens sample plus the S-Z, SNIa and local determinations. The lower shaded region indicates the  $\pm 2\text{-}\sigma$  region around the average of the  $\mathcal{L}$  lens sample for  $\Omega_m = 1.0$  and  $\Omega_\Lambda = 0.0$ . The  $1\text{-}\sigma$  error-bars indicate the statistical errors.

## 9. Conclusions

Using VLBA imaging, VLA monitoring and *Hubble Space Telescope* WFPC2 and NICMOS imaging data, we constrained mass models of the lens galaxies in the gravitational lens system B1608+656. The best mass model gives (i) an agreement between the observed and model image positions well within the observational errors, (ii) the radio flux density ratios of the images to within 10% (except for the faintest radio image) and (iii) the observed time delays (Paper I) to within 1%, although this small scatter is a coincidence.

Using the three time delays from B1608+656 (Paper I), the best isothermal mass model gives

$$H_0^{1608} = 59_{-6}^{+7} \text{ km s}^{-1} \text{ Mpc}^{-1} \quad (\Omega_m = 1, \Omega_\Lambda = 0),$$

with  $2\text{-}\sigma$  errors. When  $\Omega_m = 0.3$  and  $\Omega_\Lambda = 0.0\text{--}0.7$ ,  $H_0 = (65 - 63)_{-6}^{+7} \text{ km s}^{-1} \text{ Mpc}^{-1}$ . All models give robust values for  $H_0$ , but a systematic error of  $\pm 15 \text{ km s}^{-1} \text{ Mpc}^{-1}$  remains, due to a 20% uncertainty in the radial mass profile.

Also under the explicit assumption of the isothermal mass model, we determine the average of  $H_0$  from a sample of four lenses (B0218+357, Q0957+561, B1608+656 and PKS1830-211). We find

$$H_0^{\text{GL}} = 69 \pm 7 \text{ km s}^{-1} \text{ Mpc}^{-1} \quad (\Omega_m = 1, \Omega_\Lambda = 0),$$

with  $2\text{-}\sigma$  errors. For  $\Omega_m = 0.3$  and  $\Omega_\Lambda = 0.0\text{--}0.7$  this increases to  $H_0^{\text{GL}} = 74 \pm 8 \text{ km s}^{-1} \text{ Mpc}^{-1}$ . When including PG1115+080, these values decrease to  $64 \pm 11 \text{ km s}^{-1} \text{ Mpc}^{-1}$  and  $68 \pm 13 \text{ km s}^{-1} \text{ Mpc}^{-1}$ , respectively.

These values agree very well with the local (Freedmann et al. 1998), Type Ia Supernovae (Riess et al. 1998) and S-Z (Myers et al. 1997) determinations, supporting the reliability of the cosmological determinations of  $H_0$  from gravitational lenses. On average the lens determinations agree best with local determinations for a low density universe.

Moreover, we find that the mass model of B1608+656 is close to isothermal ( $\gamma = 0.50 \pm 0.10$ ), in good agreement with Q0957+561 and MG1654+1346. The close agreement on  $H_0$  from four out five gravitational lens systems and the agreement on  $\gamma$  from three gravitational lens systems suggest the existence of a ‘universal’ mass profile that can describe the mass distribution of spirals, ellipticals and cluster ellipticals. This profile must on average be very close to isothermal, perhaps following the profile found by Navarro, Frenk & White (1996), which is indeed close to isothermal in the intermediate region probed by lensing.

We like to thank Phillip Helbig, Ger de Bruyn & Steve Myers for giving useful comments and suggestions to improve this paper. We also like to thank Chris Lidman for providing the redshift of PKS1830-211 prior to publication. LVEK acknowledges the support from an NWO program subsidy (grant number 781-76-101). CDF acknowledges the support from an NSF grant, #AST 9420018. This research was supported in part by the European Commission, TMR Programme, Research Network Contract ERBFMRXCT96-0034 ‘CERES’.

## REFERENCES

- Bahcall, N. A., Fan, X., & Cen, R. 1997, *ApJ*, 485, L53
- Biggs, A. D., Browne, I. W. A., Helbig, P., Koopmans, L. V. E., Wilkinson, P. N., & Perley, R. A. 1999, *MNRAS*, 304, 349
- Browne, et al. 1997, in *Cosmology with the new radio surveys*, eds. M. Bremer and Jackson, N. J., p305
- Barkana, R. 1998, *ApJ*, 502, 531
- Barkana, R., Lehár, J., Falco, E. E., Grogin, N. A., Keeton, C. R., & Shapiro, I. I. 1999, *ApJ*, submitted, *astro-ph/9808096*
- Carlberg, R. G., Yee, H. K. C., Ellingson, E., Abraham, R., Gravel, P., Morris, S., & Pritchet, C. J. 1996, *ApJ*, 462, 32
- Corbett, E. A., Browne, I. W. A., Wilkinson, P. N., & Patnaik, A. R. 1996, in *Astrophysical Applications of Gravitational Lensing*, eds. C.S. Kochanek and J.N. Hewitt (Kluwer Academic Publishers: Dordrecht), p37
- Fanaroff, B. L. & Riley, J. M. 1974, *MNRAS*, 167, 31
- Fassnacht, C. D., Womble, D. S., Neugebauer, G., Browne, I. W. A., Readhead, A. C. S., Matthews, K., & Pearson, T. J. 1996, *ApJ*, 460, L103
- Fassnacht, C. 1997, *American Astronomical Society Meeting*, 191, 5903
- Fassnacht, C. D., Pearson, T. J., Readhead, A. C. S., Browne, I. W. A., Koopmans, L. V. E., Myers, S. T., Wilkinson, P. N. 1999a, *ApJ*, submitted (Paper I)
- Freedman, W. L., Mould, J. R., Kennicutt, R. C., & Madore, B. F. 1998, *astro-ph/9801080*
- Grogin, A., & Narayan, R. 1996a, *ApJ*, 464, 92
- Grogin, N. A. & Narayan, R. 1996b, *ApJ*, 473, 570
- Haarsma, D. B., Hewitt, J. N., Lehár, J., & Burke, B. F. 1999, *ApJ*, 510, 64
- Hickson, P. 1982, *ApJ*, 255, 382

- Impey, C., Falco, E., Kochanek, C., Lehar, J., McLeod, B., Rix, H.-W., Peng, C., & Keeton, C. 1998, *ApJ*, 509, 551
- Jackson, N. J., Nair, S., & Browne, I. W. A. in *Cosmology with the new radio surveys*, eds. M. Bremer, Jackson, N. J., p315
- Jackson, N., Helbig, P., Browne, I., Fassnacht, C. D., Koopmans, L., Marlow, D., & Wilkinson, P. N. 1998, *A&A*, 334, L33
- Jauncey, D. L., et al. 1991, *Nature*, 352, 132
- Kayser, R. & Refsdal, S. 1983, *A&A*, 128, 156
- Keeton, C. R., Kochanek, C. S., & Seljak, U. 1997, *ApJ*, 482, 604
- Keeton, C. R., Kochanek, C. S., & Falco, E.E. 1998, *ApJ*, 509, 561
- Keeton, C. R. & Kochanek, C. S., in *Golden Lenses: The Hubble Constant and galaxies at high redshift*, 1998, electronic Proceedings of the Workshop on Golden Lenses held at Jodrell Bank, <http://multivac.jb.man.ac.uk:8000/ceres/workshop1/proceedings.html>
- Kochanek, C. S., & Narayan, R. 1992, *ApJ*, 401, 461
- Kochanek, C. S. 1995, *ApJ*, 445, 559
- Koopmans, L. V. E., et al., 1999, *MNRAS*, 303, 727
- Kormann, R., Schneider, P., & Bartelmann, M. 1994, *A&A*, 284, 285
- Kundić, T., Cohen, J. G., Blandford, R. D., & Lubin, L. M. 1997a, *AJ*, 114, 507
- Kundić, T., et al. 1997b, *ApJ*, 482, 75
- Lidman C., Courbin, F., Meylan G., Broadhurst, T. J., Frye B., & Welch J. 1999, *ApJ*, 514, 57L
- Lovell, J. E. J., Jauncey, D. L., Reynolds, J. E., Wieringa, M. H., King, E. A., Tzioumis, A. K., McCulloch, P. M., & Edwards P. G. 1998, *ApJ*, 508, 51
- Mao, S. & Schneider, P. 1998, *MNRAS*, 295, 587

- Myers, S. T., et al. 1995, ApJ, 447, L5
- Myers, S. T., Baker, J. E., Readhead, A. C. S., Leitch, E. M., & Herbig, T. 1997, ApJ, 485, 1
- Navarro, J. F., Frenk, C. S., & White, S. D. M. 1996, ApJ, 462, 563
- Nair, S., Narasimha, D., & Rao, A. P. 1993, ApJ, 407, 46
- Patnaik, A. R., Browne, I. W. A., King, L. J., Muxlow, T. W. B., Walsh, D., & Wilkinson, P. N. 1993, MNRAS, 261, 435
- Patnaik, A. R., Porcas, R. W., & Browne, I. W. A. 1995, MNRAS, 274, L5
- Pildis, R. A., Bregman, J. N., & Evrard, A. E. 1995, ApJ, 443, 514
- Press, W. H., Teukolsky, S. A., Vetterling, W. T., & Flannery, B. P. 1992, Cambridge: University Press, —c1992, 2nd ed.,
- Refsdal, S. 1964, MNRAS 128, 307
- Refsdal, S. 1966, MNRAS 132, 101
- Riess, A. G., et al. 1998, AJ, 116, 1009
- Schechter, P.L., et al., 1997, ApJ, 475, L85
- Schechter, P.L. 1998, in Electronic Proceedings of a workshop organized by the Observatoire de Strasbourg, <http://astro.u-strasbg.fr/howfar/toc.html>
- Schneider, P., Ehlers, J., & Falco, E. E. 1992, Berlin ; New York : Springer-Verlag, [1992], 736.
- Snellen, I. A. G., De Bruyn, A. G., Schilizzi, R. T., Miley, G. K., & Myers, S. T. 1995, ApJ, 447, L9
- Tonry, J. L. 1998, AJ, 115, 1
- Tonry, J. L., & Franx, M. 1999, ApJ, 515, 512
- Van Ommen, T. D., Jones, D. L., Preston, R. A., & Jauncey, D. L. 1995, ApJ, 444, 561
- Walsh, D., Carswell, R.F., & Weymann, R.J. 1979, Nature, 279, 381

Weymann, R. J., Latham, D., Roger, J., Angel, P., Green, R. F., Liebert, J. W., Turnshek, D. A., Turnshek, D. E., & Tyson, J. A. 1980, *Nature*, 285, 641

Zehavi, I., Riess, A. G., Kirshner, R. P., & Dekel, A. 1998, *ApJ*, 503, 483